AD_____

AWARD NUMBER: W81XWH-04-1-0249

TITLE: Improved Sensitivity and Specificity for Detection of Prostate

PRINCIPAL INVESTIGATOR: Rao P. Gullapalli, Ph.D.
                         Michael Naslund, M.D.
                         John Papadimitrou, M.D.
                         Elliott Siegel, M.D.

CONTRACTING ORGANIZATION: University of Maryland Baltimore
                           Baltimore, Maryland 21201-1082

REPORT DATE: April 2006

TYPE OF REPORT: Annual

PREPARED FOR: U.S. Army Medical Research and Materiel Command
               Fort Detrick, Maryland 21702-5012

DISTRIBUTION STATEMENT: Approved for Public Release;
                        Distribution Unlimited

REPORT DOCUMENTATION PAGE

1. REPORT DATE *(DD-MM-YYYY)* 01-04-2006	2. REPORT TYPE Annual	3. DATES COVERED *(From - To)* 1 Mar 2005 – 28 Feb 2005

4. TITLE AND SUBTITLE	5a. CONTRACT NUMBER
Improved Sensitivity and Specificity for Detection of Prostate	5b. GRANT NUMBER W81XWH-04-1-0249
	5c. PROGRAM ELEMENT NUMBER

6. AUTHOR(S)	5d. PROJECT NUMBER
Rao P. Gullapalli, Ph.D.; Michael Naslund, M.D. John Papadimitrou, M.D. and Elliott Siegel, M.D.	5e. TASK NUMBER
E-Mail: rgullapalli@umm.edu	5f. WORK UNIT NUMBER

7. PERFORMING ORGANIZATION NAME(S) AND ADDRESS(ES)	8. PERFORMING ORGANIZATION REPORT NUMBER
University of Maryland Baltimore Baltimore, Maryland 21201-1082	

9. SPONSORING / MONITORING AGENCY NAME(S) AND ADDRESS(ES)	10. SPONSOR/MONITOR'S ACRONYM(S)
U.S. Army Medical Research and Materiel Command Fort Detrick, Maryland 21702-5012	
	11. SPONSOR/MONITOR'S REPORT NUMBER(S)

12. DISTRIBUTION / AVAILABILITY STATEMENT
Approved for Public Release; Distribution Unlimited

13. SUPPLEMENTARY NOTES

14. ABSTRACT

Amendment requests to the final approved HSRRB protocol were made to the local IRB on July 21, 2005 which was finally approved in August of 2005. Meanwhile the registration algorithms were tested on resected prostates available from the pathology department. Working with these prostates made it clear that the performance of the registration algorithms depended upon the accuracy with which the prostate was sliced in a parallel fashion and with uniform thickness. This led to the development of the 'prostate slicer' which allowed us to cut the prostate into uniform 3mm parallel slices. The recruitment of subjects began once the accuracy of the registration algorithms was tested to satisfaction. We have to date recruited four subjects and competed scanning on three of them. The fourth subject was claustrophobic and was unable to complete the imaging exam. We have five subjects waiting in wings to be scanned in the month of June and July. Meanwhile the IRB protocol has been submitted for renewal as it expires on June 19, 2006. No changes were made to the protocol for its renewal. In essence we have completed all requirements for Specific Aim 1 of the project. We anticipate recruiting about 5 subjects a month, which will allow us to complete the data collection before December of 2006.

15. SUBJECT TERMS
prostate, spectroscopy, MRI

16. SECURITY CLASSIFICATION OF:			17. LIMITATION OF ABSTRACT	18. NUMBER OF PAGES	19a. NAME OF RESPONSIBLE PERSON USAMRMC
a. REPORT U	b. ABSTRACT U	c. THIS PAGE U	UU	16	19b. TELEPHONE NUMBER *(include area code)*

Table of Contents

Improved Sensitivity and Specificity for Detection of Prostate
PC031042
HSRRB Log No. A-12577

Introduction

The goal of this proposal is to diagnose prostate cancer more effectively using various magnetic resonance imaging techniques available with the ultimate goal of providing information with high specificity for either treatment planning purposes or patient management. To achieve this goal we would like to address the following two specific aims.

Specific Aim 1: To estimate the efficacy of image morphing and fusion techniques required providing appropriate distortion corrections on prostate images obtained from an endorectal coil for a more accurate assessment of the correlation between MRI/MRSI and histopathology.

Specific Aim 2: The development of a tumor index based on individual MRI/MRSI characteristics through correlation with step-section histology for a more accurate determination of the tumor extent and aggressiveness.

Body

Overall Status of the Project:

Since the last report we have completed the testing and validation of Specific Aim 1. The prostate phantom built last year to test the image morphing and fusion techniques, worked very well and continues to work as a validation tool in improving our techniques. However, upon working with real prostate specimens it soon became evident that the 3mm cuts needed to be straight in order for the registration and image fusion algorithms to work well. This led us to the development of 'prostate slicer' shown in Appendix A, which holds the excised prostate and allows us to slice 3mm parallel slices in a uniform fashion before fixing the prostate for histology read. This is a major accomplishment as it (a) allows the uniform cutting of parallel slices, and (b) it does not introduce any additional errors during the registration and image fusion part of the project. We have also made some in roads into Specific Aim2. Specifically we have recruited four subjects into the study. Three of the subjects had complete exam and the fourth subject could not start the study after consenting as he found out that the MR environment was too claustrophobic. We have five additional subjects that have been contacted and three of these subjects are scheduled for MR exam during the latter part of June. Although no conclusions or prediction can be made regarding the trend of the data, the quality of the data is excellent and the results are very encouraging.   We continue to actively recruit patients and now that all our tools are in place we are shooting for about 3-5 subjects a month in order to complete the imaging part of the project by the end of 2006.

Brief Overview

MR spectroscopic information of the prostate is obtained by inserting an endorectal coil. The coils has an inflatable balloon that is typically inflated to about 100 cc in order to tightly couple with the prostate gland and avoid any involuntary motion of the gland during the imaging process. Such positioning of the coil allows one to obtain the maximum signal to noise

achievable while imaging this gland. The insertion of coil physically distorts the prostate gland and MRI/MRSI is obtained with the prostate gland in this deformed state. However, when the prostate is removed during prostatectomy, the shape of the prostate is completely different from the position when MRI/MRSI was obtained (deformed state) and also when the endorectal coil was not inserted (normal state). For accurate correlation of histology with the MRI/MRSI it becomes essential that the resected prostate be registered to the prostate in its deformed state and also the normal state (when no coil was present). To accurately characterize the prostate from the imaging findings, it is necessary to obtain 3-dimensional data that encompasses the complete prostate in vivo and then register this image set with the three dimensional images obtained from the resected prostate prior to step-sectioning. Further, the thin sections from step sectioning will need to be digitized and reconstructed as a whole prostate and registered to the in-vivo and ex-vivo images of the prostate. This will allow us to spatially correlate the imaging findings to that of the histopathology accurately. This is an exercise in morphing and registration, for which we have developed the tools and are in the process of validating. We have now completely validated these tools both on simulation phantoms and ex-vivo prostate specimens. However, during the process we discovered the need for accurate parallel cuts of the excised prostate, which led to the development of a 'prostate slicer'. A picture of the prostate slicer is shown in Appendix A. The prostate slicer allows for near precise parallel cuts of the prostate prior to fixation for histopathological evaluation. This is essential for minimizing registration and fusion errors between pathological slides and in-vivo data. We have presented our data on "Landmark-Based Elastic Registration of Magnetic Resonance Prostate Images" at 12th International Conference on Biomedical Engineering and another paper entitled "An Elastic Registration Algorithm based on Strain Energy Minimization and its Application to Prostate MR Images" at the Fourteenth International Society for Magnetic Resonance in Medicine that recently concluded in Seattle.[1,2] All papers relevant to these presentations are attached in Appendix B.

Appendix C shows typical examples of MRI results and their correlation with histopathology. Given the small sample size it is difficult to come to any conclusions at this time. We are now working on a plan to recruit 5 subjects a month for the study. Given that there are about 12-15 prostatectomy cases a month, we feel confident our surgeons feel confident that we can meet that goal.

Key Research Accomplishments

To date we have been able to do the following:

1. Build a prostate phantom for validating all registration and deformation correction algorithm.
2. Explore and quantify the performance of novel methods of elastic registration including strain energy minimization and landmark based techniques
3. Develop a prostate slicer to obtain precise parallel axial cuts of the excised prostate prior to histopathological evaluation.
4. Implement all the tools necessary for the data analysis of the prostate imaging data.
5. Validate the tools on excised prostate samples available from the pathology department.
6. Completed recruitment, imaging and evaluation of three prostate cancer patients.
7. Presented a couple of papers on elastic registration at major conferences.

Reportable Outcomes

We can currently report results from our validation of the various registration algorithms. We are currently in the process of finalizing a manuscript for submission to a major magnetic resonance journal, preferably Magnetic Resonance in Medicine or Journal of Magnetic Resonance Imaging. It is too soon to make any conclusion from the data obtained on the three patients. We can only make qualitative statements regarding the general quality of the data. So far we have been very pleased with the data in terms of the correlation between spectroscopy data and histopathological data and diffusion data and histopathological data.

Conclusions

A major accomplishment for this project has been the development of the prostate phantom. The prostate phantom as designed serves as a useful training tool for physicians as they can practice prostate biopsy and ultrasound guided radioactive seed placement during brachytherapy. The phantom can be used for quality control of spectroscopic scans. It also serves as a useful model to test registration algorithms for deformable objects. More importantly the phantom can be used to normalize prostate imaging data from different sites and also to normalize data imaging data obtained from different MR vendor's machines.

When trying to validate the registration algorithm using prostate samples from the department of pathology, it became evident that it was essential to have near perfect axial cuts of the prostate. To facilitate this we designed the 'prostate slicer', which has markedly improved our capability of matching imaging slices with the histopathology slices. We consider this a very important step in the progress of this project. This will greatly improve the quality of data as it minimizes the registration errors significantly.

We have so far completed obtaining data on three prostate cancer patients. Image data analysis and histopathological studies also have been completed. Although there is a general trend towards correlation between imaging parameters and histopathological findings, it is too early to make any judgment from this small sample size. Enrollment of subjects into the study began late due to delays from the HSRRB. In the interim we too faced the challenge of being able to slice the prostate accurately in a parallel fashion as we were generating significant errors if such a condition was not met. The development of prostate slicer has significantly alleviated this problem and we are now able to minimize errors from registration significantly.
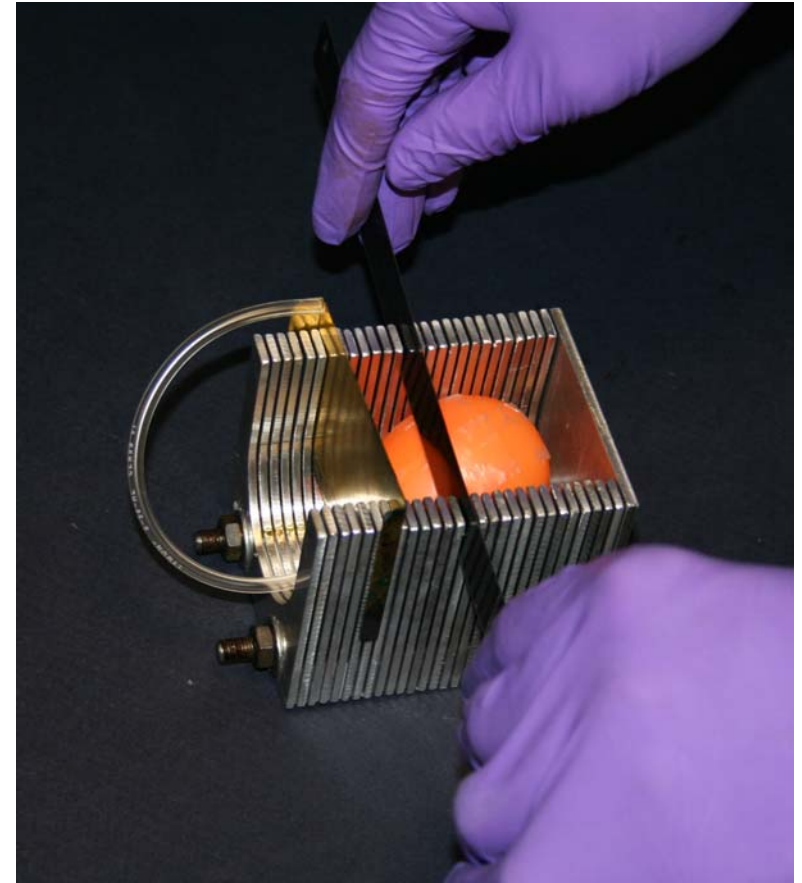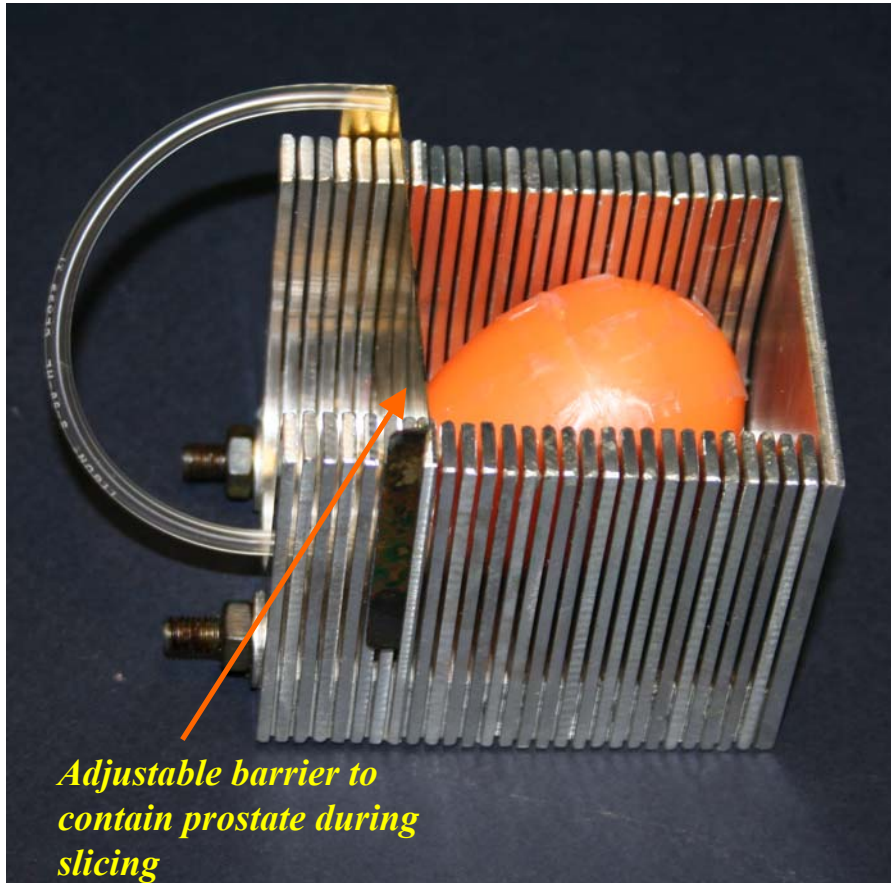
We do plan to increase our enrollment to about 5 cases a month and we feel quite confident that the data collection will be completed by the end of the year.

References:

1. Zhang B, Roys S, and Gullapalli RP. Landmark-based elastic registration of magnetic resonance prostate images. Proceedings of the International Congress of Biomedical Engineering, Singapore, 2005, p676.
2. Zhang B, and Gullapalli RP. An elastic registration algorithm based on strain energy minimization and its application to prostate MR images. Proceedings of the Fourteenth International Society for Magnetic Resonance in Medicine, Seattle, p.2979.

APPENDIX

Appendix A

Adjustable barrier to contain prostate during slicing

Prostate slicer: The slicer allows for uniform 3mm axial cuts of the prostate. One end of the slicer is fixed whereas a moveable barrier on the other end allows for various sizes of the prostate. Once the barrier is placed in position uniform slices of the prostate can be obtained using the surgical knife.

LANDMARK-BASED ELASTIC REGISTRATION OF MAGNETIC RESONANCE PROSTATE IMAGES

Bao Zhang[*], Steven Roys[*], Rao Gullapalli[*]

[*] Magnetic Resonance Research Center, Department of Radiology,
University of Maryland School of Medicine, Baltimore Maryland, U.S.A.

bzhang1@umm.edu

Abstract: The use of magnetic resonance imaging in conjunction with endorectal coil has received increased attention in the diagnosis and treatment of prostate cancer. However images and spectra obtained in this manner deform the prostate, and such deformation may lead to uncertainties in the localization of prostate cancer during therapy. We propose a landmark-based elastic image registration procedure to address this problem. This procedure consists of two steps. The first step requires the identification of feature landmarks (points, curves or surfaces) from the source and target images. The second step finds the transformation through the use of a novel registration algorithm that is based on the minimization of a physically motivated energy function, namely, the strain energy. Gauss-Seidel method was used in the numerical implementation of the novel registration algorithm. This registration procedure was validated on synthetic prostate phantom image data. The registration accuracy was 1.0 ± 0.6 pixels. Further validation was also performed on 6 cases of actual MR prostate images. The corrected deformed images showed excellent correspondence with the undeformed ones in all cases. The registration results on synthetic phantom, and prostate data in vivo demonstrated that the registration procedure was significant to prostate cancer diagnosis, staging and treatment planning.

Introduction

MR imaging of the prostate using the endorectal coil (erMRI) is considered to be state-of-the-art technique for diagnosing prostate cancer [1]. The endorectal coil provides images with superior signal to noise and image quality compared to images taken from a body array coil. However, the insertion of the endorectal coil with subsequent inflation of the balloon that encases the coil, results in the distortion of the prostate gland. The inflation of the balloon with as much as 100cc of air is necessary for the coils to be coupled with the prostate gland and it helps to keep the prostate gland from moving. Although images and MR spectra are obtained in this deformed stage, treatment however may take place with the prostate in its undeformed state. Registration of the deformed prostate images to the undeformed images becomes a necessary task for any interventional procedure or for radiation treatment planning.

Image registration is a procedure of determining a one-to-one transformation between two image spaces which maps each pixel/voxel in one space onto the corresponding pixel/voxel in another space. According to the underlying transformation, image registration can be classified into two categories: rigid and non-rigid registration. Rigid registration deals with the translation and rotation of images [2]. Non-rigid registration, on the other hand deals with the cases that rigid registration can not handle. In some simple cases such as scaling, affine transformation, and perspective projection, the underlying transformation is a global function of positions with some parameters which can be optimized by minimizing (or maximizing) the cost functions. Under certain circumstances, however, these global transformation functions are not sufficient to depict the local image deformation. New transformation functions are then introduced. Polynomials and radial basis functions (RBF) are two most often used functions to solve this problem [3, 4] as they are able to handle even locally varying geometric distortions.

Besides the registration methods in which the transformations are defined as explicit functions of position coordinates, there are some other non-rigid registration methods in which the transformations are solutions of some governing equations. Such registration methods include elastic registration, fluid registration, diffusion-based registration, and optical flow based registration. [5] Among these non-rigid registration methods, elastic registration is of particular interest in medical image registration since it takes into account the physical properties of the image transformation.

Traditional elastic image registration schemes derive forces from image data using some similarity measure and then deform the source image into target [6-8]. Instead of computing the forces and solving Navier-Lame equation for deformation, the proposed registration algorithm in this paper models the images as a dynamical system and derives the deformation utilizing the principle of strain energy minimization, a special case of Lagrange equation.

Materials and Methods

The proposed registration procedure consists of 2 steps. The first step manually identifies feature landmarks (points, curves or surfaces) from the source and target images. The second step finds the

transformation through the use of a novel registration algorithm that is based on the minimization of a physically motivated energy function, namely, the strain energy. The landmark-based registration procedure is illustrated in Fig. 1.

According to the principles of dynamics, the potential energy function has a stationary value if the system is conservative and is in equilibrium. Especially, if the system is stable, then the potential energy function is minimized. The theorem can be applied to prostate erMRI to derive the underlying deformation.

Treating the prostate as an elastic body, the potential energy of the system is purely the strain energy. It is defined as following [9]:

$$U = \iiint_V \frac{1}{2}\left[\lambda e^2 + 2G(\varepsilon_x^2 + \varepsilon_y^2 + \varepsilon_z^2) + G(\gamma_{xy}^2 + \gamma_{yz}^2 + \gamma_{xz}^2)\right]dV$$

where, λ and G are Lame constants characterizing material constitutive properties, ε_i ($i = x$, y or z) is the normal strain in i direction, γ_{ij} ($ij = xy$, yz or xz) is the shear strain in i plane pointing to j direction, e is the unit volume change, and V is the volume.

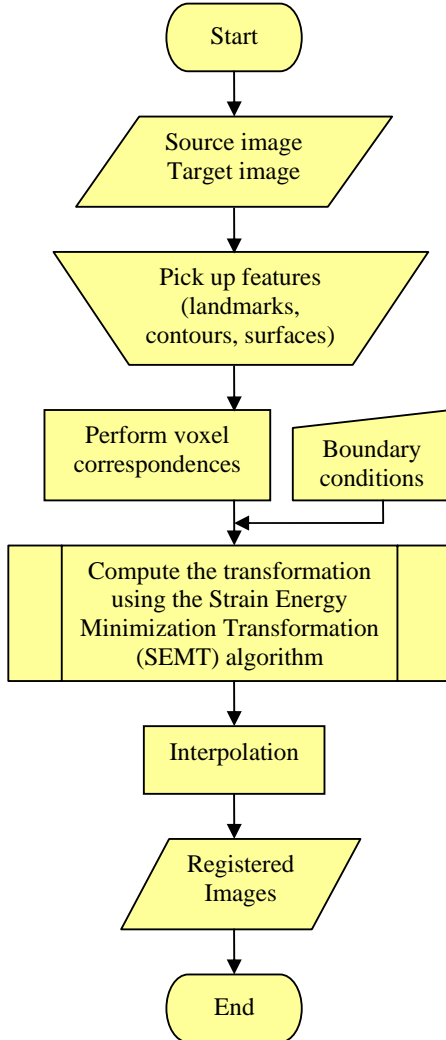Assuming that the prostate is incompressible, which means that e is zero, the above equation is simplified as:

$$U = G\iiint_V \left[(\varepsilon_x^2 + \varepsilon_y^2 + \varepsilon_z^2) + \frac{1}{2}(\gamma_{xy}^2 + \gamma_{yz}^2 + \gamma_{xz}^2)\right]dV$$

The strain energy minimization requires:

$$\frac{\partial U}{\partial x_i} = \frac{\partial U}{\partial y_i} = \frac{\partial U}{\partial z_i} = 0 \qquad (1)$$

Relating the strain ε with the displacement u by the strain-displacement relationship, the displacement distribution that satisfies Eqn (1) can be expressed, in terms of positions (X_{ijk}, Y_{ijk}, Z_{ijk}), as [9]:

$$
\begin{aligned}
X_{ijk} &= \frac{\left[\begin{array}{c}2X_{i+1jk} + 2X_{i-1jk} + X_{ij+1k} + X_{ij-1k} + X_{ijk+1} + X_{ijk-1} + (Y_{i+1jk} - Y_{ijk}) \\ -(Y_{i+1j-1k} - Y_{ij-1k}) + (Z_{i+1jk} - Z_{ijk}) - (Z_{i+1jk-1} - Z_{ijk-1})\end{array}\right]}{8} \\[8pt]
Y_{ijk} &= \frac{\left[\begin{array}{c}Y_{i+1jk} + Y_{i-1jk} + 2Y_{ij+1k} + 2Y_{ij-1k} + Y_{ijk+1} + Y_{ijk-1} + (Z_{ij+1k} - Z_{ijk}) \\ -(Z_{ij+1k-1} - Z_{ijk-1}) + (X_{ij+1k} - X_{ijk}) - (X_{i-1j+1k} - X_{i-1jk})\end{array}\right]}{8} \\[8pt]
Z_{ijk} &= \frac{\left[\begin{array}{c}Z_{i+1jk} + Z_{i-1jk} + Z_{ij+1k} + Z_{ij-1k} + 2Z_{ijk+1} + 2Z_{ijk-1} + (X_{ijk+1} - X_{ijk}) \\ -(X_{i-1jk+1} - X_{i-1jk}) + (Y_{ijk+1} - Y_{ijk}) - (Y_{ij-1k+1} - Y_{ij-1k})\end{array}\right]}{8}
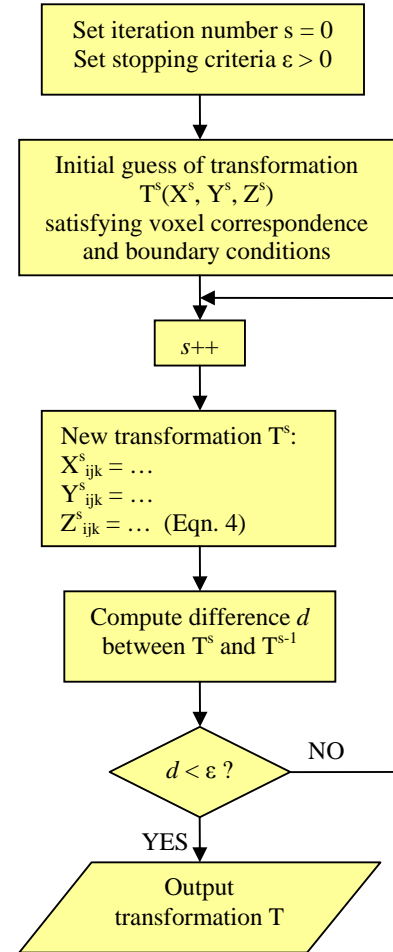\end{aligned}
\qquad (2)
$$

Fig. 1: Flowchart of the registration procedure and SEMT algorithm implemented using Gauss-Seidel method.

Note, that in the above solutions, the new position $(X_{ijk}, Y_{ijk}, Z_{ijk})$ is always explicitly expressed by its closest neighbors. The computation of $(X_{ijk}, Y_{ijk}, Z_{ijk})$ can be easily implemented using Gauss-Seidel method. The numerical implementation of strain energy minimization transformation (SEMT) was also illustrated in Fig. 1.

Results

This registration algorithm was tested on numerical simulation and phantom images first, and then applied to actual prostate images. The preliminary results are depicted below.

Numerical simulation   In the numerical simulation, a sphere (radius, 10) is elastically deformed to an ellipsoid (the three semiaxes: a=9, b=12, and c=10 in x,y and z direction respectively) along with the embedded 3D character F. Both the sphere and the ellipsoid are located at the center of a 30×30×30 volume. Figure 2 illustrates the geometric shapes of the sphere and the ellipsoid.
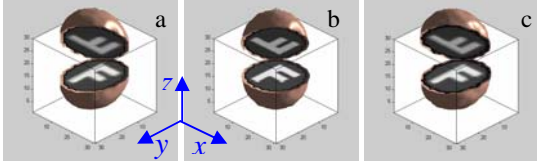

Fig. 2: The 3D geometric shape of (a) the target (reference) ellipsoid, (b) the source sphehre, and (c) the registered volume from source to target, with a 3D character 'F' in it. The Cartesian coordinate system *xyz* is shown for later reference.

As shown in Fig. 2, the brown surfaces of the source ball and the target ellipsoid are manually picked by the user to serve as landmarks for the elastic registration.

Figure 3 illustrates the registration results in 3 orthogonal planes. The first row shows the results in *xy* plane; the second row, *yz* plane; and the third row, *xz* plane. The first column shows the target (or, reference) images in three orthogonal planes respectively; the second column shows the source images; the third column shows the registered images; the forth row shows the intensity difference between the source and target images; and the fifth column shows the intensity difference between the target and registered images. Comparing the image differences as shown in Fig. 3 column 4 and column 5, we found that the registered image is much more similar to the reference than the source image.

We also computed the normalized cross correlation (NCC) to evaluate the performance of the registration algorithm. It was improved from 0.91 to 1.00 by the registration.

Also shown in Fig. 3 is the displacement distribution along the three planes, which is superposed to the source images in the second column. The displacement vector is represented by a blue arrow, where its direction is the direction of the displacement, and its magnitude is the length.

Fig. 3: The registration results in three orthogonal central planes.

Prostate phantom   A prostate phantom was constructed to quantitatively validate this algorithm. [10] The phantom was scanned using a 1.5T Siemens scanner before and after the inflation of the endorectal balloon with 100cc air. The prostate phantom is in equilibrium while scanning so its strain energy has a stationary value and equation 2 can be applied to the registration.

The image size was 256×256×29, and the resolution was 0.625×0.625×2.5 mm.

Figure 4 shows the segmented prostate phantom before and after deformation, and the registered volume as well. The similarity measure showed that NCC was improved from 0.84 to 0.99.
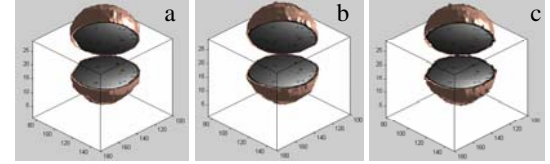

Fig. 4: The segmented a) source, b) target, and c) registered prostate phantom. The dark spots shown in the open plane are sesame seeds randomly distributed in the phantom.

Table 1: Positions of 12 markers in the source, target and registered images, and the respective displacement, and registration error.

Seeds	Position (pixel)			Distance (pixel)	
	Source	Target	Registered	Source to target	Target to registered
P1	(130,170)	(130,174)	(130,175)	4.0	1.0
P2	(126,157)	(126,162)	(125,161)	5.0	1.4
P3	(119,160)	(119,165)	(120,165)	5.0	1.0
P4	(117,161)	(115,165)	(116,165)	4.5	1.0
P5	(140,150)	(140,155)	(140,154)	5.0	1.0
P6	(135,139)	(135,144)	(135,144)	5.0	0.0
P7	(130,138)	(130,143)	(130,142)	5.0	1.0
P8	(107,141)	(107,146)	(106,146)	5.0	1.0
P9	(141,131)	(141,136)	(139,135)	5.0	2.2
P10	(134,127)	(133,132)	(133,132)	5.1	0.0
P11	(125,126)	(124,131)	(123,131)	5.1	1.0
P12	(121,128)	(120,132)	(120,133)	4.1	1.0

The sesame seeds in the phantom served the purpose of landmarks to evaluate the registration algorithm. Table 1 lists the positions of 12 sesame seeds in the source, target and registered images, the displacement (measured as the position difference of seeds between the source and target), and the registration error (measured as the position difference of seeds between the target and registered images). The overall displacement in magnitude (mean±stdev) is 4.8±0.4 pixels. The registration error is 1.0±0.6 pixels (or 0.6±0.4 mm). These results quantitatively demonstrated the excellent performance of the registration algorithm.

Actual prostate data   In the case of actual prostate volume registration, erMRI was conducted on a patient before and after the inflation of the balloon with 40 cc air. The image size was 256×256×25, and the resolution was 0.625×0.625×3.5 mm.

Figure 5 illustrates the segmented prostate images before deformation, after deformation, and registered. The similarity measure shows that NCC was improved from 0.62 to 0.98 by the registration.
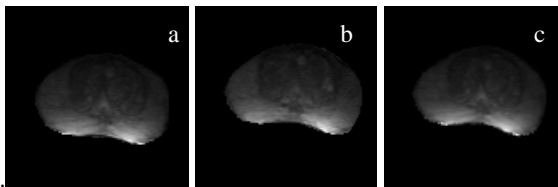

Fig. 5: The segmented a) source, b) target, and c) registered prostate volume.

Discussions and Conclusions

We have developed a novel SEMT algorithm to perform prostate image registration. The algorithm requires the subject under investigation to be elastic and stable. So organs such as breast and prostate can benefit from this method as they satisfy this requirement.

The transformation matrix obtained by SEMT relies on the landmark correspondences. Any mismatch of the correspondences may incur global registration errors. It is crucial to maintain the accuracy of landmark correspondence as high as possible. Active contour and/or active surface models may be adopted to generate the correspondences such that the error is at sub-pixel level [11, 12].

Although the transformation matrix is for the whole data volume in our algorithm, it is only valid in VOI. Outside that region, the deformation is erroneous. While some differences in the mechanical property of the tissue is expected, dramatic differences in the mechanical properties are not handled well by the SEMT algorithm. This is reasonable since in the SEMT algorithm, the equation we used to compute the voxel position is parameter free (see Eqn. 2). So a subtle assumption is the material has a constant mechanical property.

Generally it is difficult to quantitatively evaluate the performance of a registration algorithm in most situations because of the lack of 'ground truth'. With the help of the constructed prostate phantom, the registration error was quantitatively obtained (see Table 1).

In conclusion, a novel registration algorithm based on a physically meaningful transformation was implemented. This algorithm was tested on synthetic phantom and actual clinical data respectively. The results from synthetic and phantom data showed that the accuracy of our registration is within 1 pixel. The clinical prostate data showed the feasibility of the registration algorithm to prostate imaging.

References
1. Schnall MD, Imai Y, Tomaszewski J, Pollack HM, Lenkinski RE, Kressel HY, Prostate cancer: local staging with endorectal surface coil MR imaging, *Radiology* 1991; 178: 797-802.
2. Fitzpatrik J.M., West J.B., The distribution of target registration error in rigid-body point-based registration, *IEEE transactions on medical imaging* 20 (2001) 917-927
3. Wu X, Dibiase SJ, Gullapalli R, Yu CX, Deformable image registration for the use of magnetic resonance spectroscopy in prostate treatment planning, *Int J Radiat Oncol Biol Phys*. 2004 Apr 1;58(5):1577-83
4. Lian J, Xing L, Hunjan S, Dumoulin C, Levin J, Lo A, Watkins R, Rohling K, Giaquinto R, Kim D, Spielman D, Daniel B Mapping of the prostate in endorectal coil-based MRI/MRSI and CT: a deformable registration and validation study, *Med Phys*. 2004 Nov;31(11):3087-94
5. Barbara Zitova B., Flusser J., Image registration methods: a survey, *Image and Vision Computing* 21 (2003)977-1000
6. Broit C., Optimal registration of deformed images. PhD thesis, Compter and information science, University of Pensylvania, 1981.
7. Davatzikos C. Prince J.L. Bryan R.N. Image registration based on boundary mapping, *IEEE Trans. on Medical Imaging* 15 (1996) 112-115.
8. Peckar W. Schnorr C., Rohr K., Stiehl H.S., Two step parameter-free elastic image registration with prescribed point displacements, *J. of mathematical imaging and vision* 10 (1999) 143-162
9. Ugural AC, Fenster SK, Advanced Strength and Applied Elasticity 3rd ed. pp1-90, Prentice-Hall, Inc, New Jersey, 1995
10. Zhang B., Rao P. Gullapalli RP, multi-purpose prostate phantom, *ISMRM* 2005
11. Kass M., Witkin A., and Terzopoulos D., ``Snakes: Active Contour Models''. International *Journal of Computer Vision*, 1:321-331, 1988
12. Cohen L. and Cohen I. Finite-Element Methods for Active Contour Models and Ballons for 2D and 3D Images. *IEEE Transactions on Pattern Analysis and Machine Intelligence*, 15(11):1131-1147, November 1993

An Elastic Registration Algorithm based on Strain Energy Minimization and its Application to Prostate MR images

B. Zhang[1], R. P. Gullapalli[1]

[1]Magnetic Resonance Research Center, Dept of Radiology, University of Maryland School of Medicine, Baltimore, MD, United States

Background

Magnetic resonance imaging using the endorectal coil (erMRI) has become the clinical standard in the diagnosis of prostate cancer as it provides excellent quality high resolution images. However the images and spectra obtained using the endorectal coil experience certain amount of displacement from their original position and the prostate is imaged in this displaced, distorted position. Such displacement and distortion during diagnosis leads to uncertainties in the localization of prostate cancer during therapeutic intervention as in the case of radiation therapy. Image registration is a necessary exercise to transform the diagnostic images to their undistorted state. Rigid body registration is inadequate since the prostate encounters non-rigid elastic deformation. Elastic registration is of particular interest in erMRI since it takes into account the physical process that prostate has experienced during the medical imaging procedure. Traditional elastic image registration schemes derive forces from image data using some similarity measure and then deform the source image into target. [1,2] Instead of computing the forces and solving the Navier-Lame equation for deformation, the proposed registration algorithm in this work models the image as a dynamic system in equilibrium and derives the deformation using the principle of strain energy minimization.

Method

Strain Energy Minimization According to the principles of dynamics, the potential energy function has a stationary value if the system is conservative and is in equilibrium. Especially, if the system is stable, then the potential energy function is minimized. [3] In prostate erMRI, the prostate is in equilibrium before and after the insertion of endorectal coil, hence the above theorem can be applied to derive the underlying deformation within the prostate.

Treating the prostate as an incompressible elastic body, the potential energy function is purely the strain energy U. It is defined as

$$U = G \iiint \left[\left(\frac{\partial u}{\partial x} \right)^2 + \left(\frac{\partial v}{\partial y} \right)^2 + \left(\frac{\partial w}{\partial z} \right)^2 \right] dxdydz + \frac{1}{2} G \iiint \left[\left(\frac{\partial u}{\partial y} + \frac{\partial v}{\partial x} \right)^2 + \left(\frac{\partial v}{\partial z} + \frac{\partial w}{\partial y} \right)^2 + \left(\frac{\partial u}{\partial z} + \frac{\partial w}{\partial x} \right)^2 \right] dxdydz$$

where G is the shear modulus characterizing the prostate constitutive property, u, v, and w are displacements in x, y, and z directions, respectively. The strain energy minimization requires $\delta U = 0$. The boundary conditions of this problem are of the Dirichlet boundary form:

$$\vec{u} \mid_{\partial \Omega 1} = \vec{u}(u,v,w) \mid_{\partial \Omega 1} = 0 \text{ and } \vec{u} \mid_{\partial \Omega 2} = \vec{u}(u,v,w) \mid_{\partial \Omega 2} = (u(x,y,z), v(x,y,z), w(x,y,z)) \mid_{\partial \Omega 2}$$

where $\partial \Omega 1$ denotes the outer boundary of the data volume and $\partial \Omega 2$ denotes the surface of the prostate.

Discretization Using the forward difference formula for first derivative of displacement, the strain energy minimization equation can be expressed in discrete form as a function of pixel positions (X_{ijk}, Y_{ijk}, Z_{ijk}):

$$X_{ijk} = \frac{\left[2X_{i+1jk} + 2X_{i-1jk} + X_{ij+1k} + X_{ij-1k} + X_{ijk+1} + X_{ijk-1} + (Y_{i+1jk} - Y_{ijk}) - (Y_{i+1j-1k} - Y_{ij-1k}) + (Z_{i+1jk} - Z_{ijk}) - (Z_{i+1jk-1} - Z_{ijk-1}) \right]}{8}$$

$$Y_{ijk} = \frac{\left[Y_{i+1jk} + Y_{i-1jk} + 2Y_{ij+1k} + 2Y_{ij-1k} + Y_{ijk+1} + Y_{ijk-1} + (Z_{ij+1k} - Z_{ijk}) - (Z_{ij+1k-1} - Z_{ijk-1}) + (X_{ij+1k} - X_{ijk}) - (X_{i-1j+1k} - X_{i-1jk}) \right]}{8}$$

$$Z_{ijk} = \frac{\left[Z_{i+1jk} + Z_{i-1jk} + Z_{ij+1k} + Z_{ij-1k} + 2Z_{ijk+1} + 2Z_{ijk-1} + (X_{ijk+1} - X_{ijk}) - (X_{i-1jk+1} - X_{i-1jk}) + (Y_{ijk+1} - Y_{ijk}) - (Y_{ij-1k+1} - Y_{ij-1k}) \right]}{8}$$

Combining the discretized boundary conditions, the final position can be determined.

Numerical Implementation

Note, that in the above solutions, the new position (X_{ijk}, Y_{ijk}, Z_{ijk}) is always explicitly expressed by its closest neighbors. This particular form of solution suggests that Gauss-Seidel method can be directly used for the computation of (X_{ijk}, Y_{ijk}, Z_{ijk}).

Data Acquasition The prostate phantom and patient data were acquired on Philips Eclipse 1.5T system. The prostate phantom was built in-house and incorporates all the necessary elements of a prostate gland including the tissue consistency, and the biochemicals contained within a normal prostate tissue.[4] The prostate phantom also has incorporated within it seeds that serve as landmarks and are helpful in assessing the accuracy of registration. The image size of the prostate phantom was 256×256×29, and the resolution was 0.625×0.625×2.5 mm. T2-wieghted images (256x256x25) of the prostate were obtained from patients with the endorectal coil in its fully inflated position and completely deflated position at a TE of 110ms and a TR of 3500ms at a voxel resolution of 0.625×0.625×3.5 mm.

Results

Figure 1 displays the representative resulting images from the registration along with the displacement vectors. The registration error was found to be 1.0±0.6 pixels (or 0.6±0.4 mm) for displacements ranging from 4-6mm due to the insertion of the coil. These results quantitatively demonstrated the excellent performance of the registration algorithm. Representative images from a patient's prostate are shown in figure 2. The similarity measure shows that normalized correlation coefficient improved from 0.62±0.12 to 0.98±0.08 by the registration.

Conclusion

In conclusion, a novel registration algorithm based on a strain energy transformation was implemented. This algorithm was tested on phantom and actual clinical data respectively. The results from phantom data showed that the accuracy of our registration is within 1 pixel. The clinical prostate data showed the feasibility of the registration algorithm to prostate imaging.

References

1. Davatzikos C. et al., *IEEE Trans on Medical Imaging* 15 (1996) 112-115.
2. Peckar W. et al., *J. of mathematical imaging and vision* 10 (1999) 143-162.
3. Greenwood DT, Classical Dynamics, Dover, 1997.
4. Zhang B, Gullapalli RP, Proc of ISMRM (2005) pp2115.

Fig. 1: Representative registration results for prostate phantom images. (a) reference image (b) source image overlapped with the displacement obtained. (c) registered image. (d) difference between the segmented reference and source. (e) difference between the segmented reference and the registered image.
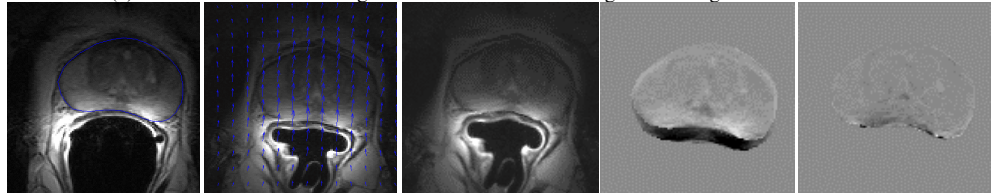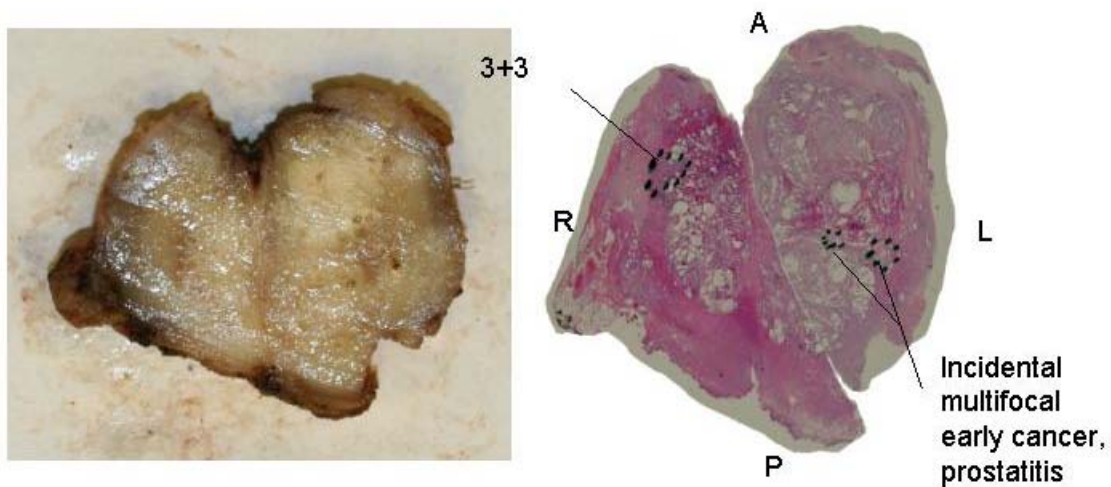

Fig. 2: Representative registration results for actual prostate images. (a) reference image (b) source image overlapped with the displacement obtained. (c) registered image. (d) difference between the segmented reference and source. (e) difference between the segmented reference and the registered image.
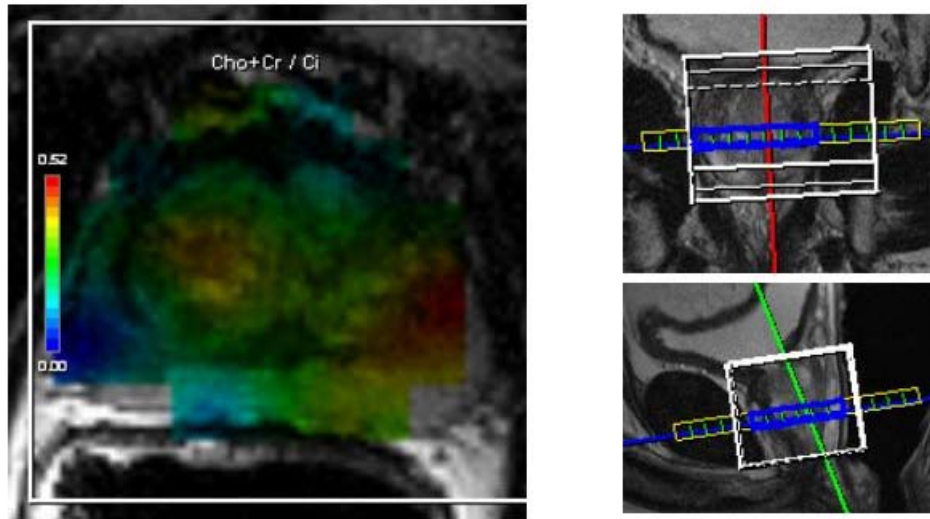
Appendix C

MRI Results

Prostate specimen & Histopathology

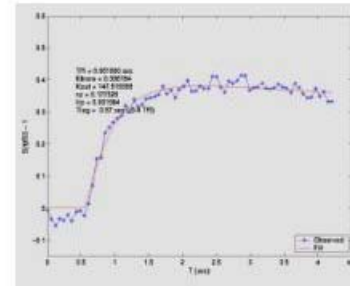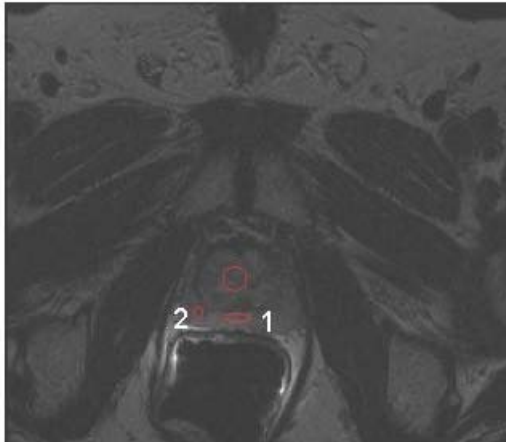One of the prostate slices along with H&E stained specimen with findings marked by the pathologist
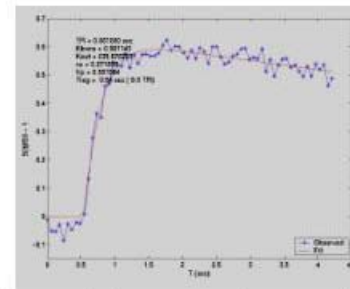
Spectroscopy image

Ratio map of Cho+Cr/Ci

Spectroscopic findings from the same location as in the previous histological slide. Abnormal areas shown in red.

Dynamic Contrast Enhanced Study

PZ 1

PZ 2

Uptake curves from dynamic contrast enhanced images along with Parameters from two compartment kinetic modeling. Region 2 shows increased permeability compared to region 1 in the peripheral zone which compares with histopathology (not shown).